Real-Time Moire Interferometry

H. S. Johnson *J. A. Gilbert*

Department of Mechanical Engineering
University of Alabama-Huntsville
Huntsville, Alabama 35899

D. R. Matthys

Department of Physics
Marquette University
Milwaukee, Wisconsin 53233

T. D. Dudderar

AT&T Bell Laboratories
Murray Hill, New Jersey 07974

ABSTRACT

A high frequency moire interferometry technique to continuously monitor in-plane surface displacement is presented. This approach employs fiber optics and a thermoplastic device to holographically record the initial carrier pattern produced on the surface of a test specimen. The carrier is modulated as the specimen deforms and moire fringes, indicative of in-plane displacement, are observed in real time. Unwanted holo-interferometric patterns are eliminated by appropriately adjusting the polarization of the reference wavefront. This paper describes a demonstration of the real-time technique as applied to the study of deformations in a notched beam subjected to a three point loading.

1. INTRODUCTION

High frequency moire interferometry is a highly sensitive full-field optical method useful for measurement of surface displacement [1-3]. The technique requires that a reflective, high-frequency phase-type grating be transferred from a mold to the surface of the specimen. The latter is produced by exposing a photographic plate to the standing wave interference pattern produced at the intersection of two plane coherent wavefronts. Photographic processing and drying of the plate results in non-uniform shrinkage of the gelatin, producing a regularly corrugated mold shaped by the pattern of equispaced straight and parallel interference fringes. A thin film of reflective material is deposited on the surface of the mold in a vacuum chamber. This coated surface is then epoxied to the surface of test specimen. Once the epoxy has cured, the mold is removed, leaving the reflective, high-frequency phase grating on the test surface. Where appropriately illuminated, the interference of the latter with a reference grating having twice the spatial frequency yields a moire pattern that can be analyzed to measure a selected component of surface displacement.

In practice, aberrations or pre-load prevent the grating, once bonded to the surface of the specimen, from being perfect (i.e., composed of perfectly straight, uniformly spaced corrugations) and a few fringes may be observed in the initial field when it is interrogated by the reference grating. This process may also contribute to the initial fringe pattern if the wavefronts of the two interfering beams used to create the reference grating are themselves not perfectly plane. Fortunately, introducing a carrier fringe pattern prior to loading permits these initial "no-load" fringes to be optically subtracted from the load-induced displacement fringe pattern. There are two conditions that have been discussed [4] in which this subtraction may not be necessary: (1) when the initial "no-load" fringe pattern is sparse but the full-load pattern has high fringe density, or (2) when the field of view has been magnified to such an extent that the initial pattern, as seen in the field of view, is a fraction of a fringe order. Only cases that satisfy one of these conditions have been studied in "real-time" (where the investigator is able to continuously monitor and evaluate full-field displacement at any point during the loading process); other cases involving relatively slight loading, and consequently only a modest number of fringes in the final state, have required that the double exposure technique be used to optically subtract the initial fringes from the field of view.

This study shows that holographic techniques can be used to store the initial carrier pattern for real-time analysis in the most general case. Fiber optic components are incorporated into the experimental set-up used to obtain the mold and into the displacement recording system to provide greater flexibility and potential optical access to remote test locations.

2. INTERFEROMETRIC MOIRE

2.1 Analysis

In high frequency moire interferometry the surface displacement may be related to the moire fringe pattern by the equation

$$U = (1/f)\, N \qquad 1$$

where U is the displacement component measured perpendicular to the lines in the reference grating, f is the spatial frequency (the reciprocal of the distance between lines in the reference grating, usually defined as its pitch, p), and N is the order number assigned to fringes in the pattern. The reference grating (also called the virtual grating) is created in space by two interfering plane wavefronts (say W and W_1) of coherent light (see Figure 1). The frequency of the interference lines, f, depends on the angle of intersection between the normals to the wavefronts, (shown as 2α), and is characterized by the equation:

$$f = (2 \sin \alpha) / \lambda \qquad 2$$

where λ is the wavelength of the incident light.

The substitution of Equation 2 into Equation 1 gives an expression for the in-plane displacement component, U, measured in a direction perpendicular to the lines in the reference grating,

$$U = N \lambda / 2 \sin \alpha \qquad 3$$

in terms of the fringe order number, N, the wavelength of light, and the angle of wavefront interference.

2.2 Mold and Grating Production

Figure 2 shows the optical configuration used to produce the mold for the high frequency grating. The flat mirror and photographic plate (shown as 5 and 6 on that figure) were illuminated by a collimated beam of argon ion laser light (wavelength = 514.5 nm) generated by positioning the exit end of a monomode fiber at the focal point of a parabolic mirror. The resulting collimated beam of coherent light was used to illuminate the photographic plate both directly (beam A) and reflected off a flat mirror (beam B). In the set-up shown in Figure 2 each beam made an angle of 18 degrees with respect to the normal to the photographic plate. This configuration produced a virtual grating of equispaced vertical lines with a spatial frequency (governed by Equation 2) of approximately 1200 lines/mm.

After a first simultaneous exposure to beams A and B, the photographic plate was rotated 90 degrees around an axis normal to the surface and exposed for a second time. This procedure produced the cross grating necessary for complete in-plane displacement analysis (although the present investigation focuses on recording a single displacement component).

Commercially available high resolution photographic plates were used to record the phase grating. Exposures were made using the energy controlled mode of the shutter system. A light sensing detector was placed in the collimated light beam outside of the field used to illuminate the photographic plate. The light intensity falling on the detector was scaled by an appropriate sampling factor which related the intensity monitored by the detector to that actually illuminating the photographic plate. The system was then operated to automatically assure exposures of optimum† integrated intensity.

Aluminum and gold have been shown to be good reflective mold overcoats because of their high reflectivity as thin films, low adhesion to the developed plate, and resistance to tarnishing [4]. Since the high availability and low cost of aluminum made it more desirable for testing, an aluminum overcoat approximately 1000 angstroms thick (50% reflectance) was vapor deposited on the plate in an environmentally controlled chamber. As illustrated in Figure 3 and discussed in the Appendix, this aluminum grating was then transferred to the surface of the specimen shown in Figure 4.

3. EXPERIMENTAL

3.1 Set-up

Figure 5 shows the experimental set-up used to observe and record real-time moire interferograms. The light beam from an argon ion laser, item 1, was split into two parts to form the object illumination and reference beams required for holographic recording. Each beam was launched into a separate single mode step-index fiber [5,6] used to reduce stray illumination, improve flexibility and simplify the optical system.

The exit end of the object illumination fiber, 4, was placed at the focal point of a parabolic mirror, 6, (2 m focal length, 0.41 mm diameter), producing a wide collimated beam of coherent light. The parabolic mirror directed this object beam towards the specimen holder assembly, 7, where a flat mirror, 8, was positioned at 90 degrees to the model. This portion of the optical set-up was identical to that used to generate the mold. Rotation of the entire assembly about a vertical axis controlled the frequency of the virtual grating formed by the interference of the direct beam, A, and the reflected beam, B. The orientation of the stage was chosen to interrogate the specimen with a virtual grating having a frequency twice that of the real grating.

The specimen was placed in its holder under slight pre-load. After rotating the assembly the specimen grating was oriented such that the +1 diffraction order of beam A coincided with the −1 diffraction order of beam B. With this alignment light was diffracted in a direction normal to the surface as illustrated in Figure 6 (extracted from Reference [4]).

† It was found that two exposures, of 1100 ergs/sq cm each, produced a cross grating with the largest first order transmission diffraction efficiency.

The remaining optical components of the set-up were positioned along this direction as follows: (1) A linear polarizer was placed in the path of the diffracted wavefronts at location 10 (see again Figure 5) so as to polarize them vertically for maximum holographic diffraction efficiency. (2) These polarized wavefronts passed through a 38.1 mm diameter, imaging lens of 375 cm focal length positioned at location 11 (56.25 cm from the test surface) to produce a magnification of two at image plane (location 13). (3) A thermoplastic holographic recording device was placed normal to the direction of propagation at location 12, 15 cm behind the focal point of the lens. The diffracted wavefronts were then stored holographically and real images of the object and reconstructed holograms were then recorded in the image plane (location 13) on polaroid or regular film.

Light exiting from the reference fiber passed through a half wave plate, 9, and polarizer, 10, before illuminating the thermoplastic hologram plate at 12. The half wave plate and polarizer combination provided variable light transmission in a preferred direction of polarization while a detector mounted behind the thermoplastic plate (not shown in Figure 5) enabled exposures to be regulated automatically using the shutter system in an energy controlled mode.

3.2 Procedure and Results

The notched beam demonstration specimen was placed in the loading frame with its longitudinal axis in the oriented horizontally as shown in Figure 7. A carrier fringe pattern was created by introducing a linear mismatch between the object and virtual gratings. Ideally, carrier fringes should be straight lines of equal density. Unfortunately, however, an initial pre-load was required to hold the model in place. This initial deformation, coupled with irregularities in the real grating distorted the carrier fringe pattern, especially in the region of high strain (near the notch) as shown in Figure 8. A hologram of the carrier pattern was recorded with polarizations of object and reference beams aligned in the vertical direction. Relative intensities of the two beams were adjusted using the variable density beam splitter located at location 2. A holographic reconstruction of the object surface with the initial carrier fringe pattern was then photographed in the image plane by blocking the object beam and suitably illuminating the hologram (again see Figure 8).

A real-time response was observed when the notched beam was loaded by displacing the lower supports. Figure 9 shows the modulated carrier pattern with the lower supports displaced 7.62×10^{-3} mm (0.0003 in.) upwards. In this case the reference beam was blocked so as to display only the loaded state. When the initial and the modulated states were reconstructed simultaneously, two holographic fringe patterns (resulting from the dual beam illumination) and two sets of carrier fringes (caused by the superposition of the two diffracted wavefronts in the loaded and unloaded condition) appeared, resulting in a superposition much too complicated to analyze. However, each holographic fringe pattern could be reconstructed independently by successively blocking the reflected and direct beams. Figures 10 and 11 show the patterns recorded with beams A and B, respectively. Of course, each holographic fringe pattern is superimposed on the initial carrier.

The holographic fringe patterns are characterized by the expression

$$\underline{g} \cdot \underline{d} = n_d \lambda \qquad 4$$

where $\underline{g}$ is the sensitivity vector $(\underline{k}_2 - \underline{k}_1)$, $\underline{\bar{k}}_2$ and $\underline{\bar{k}}_1$ are unit vectors in the illumination and observation directions respectively, $\underline{d}$ is the displacement at the surface observation point, n_d is the fringe order number, and λ is the wavelength. The sensitivity vector, g_A, of the pattern recorded with direct illumination (beam A) is described by

$$g_A = \underline{\bar{k}}_2 - (-\sin\alpha \underline{i} - \cos\alpha \underline{k}) \qquad 5$$

while the sensitivity vector, g_B, of the pattern recorded with reflected illumination (beam B) is described by

$$g_B = \underline{k}_2 - (\sin\alpha\underline{i} - \cos\alpha\underline{k}) \; . \qquad 6$$

where α is the angle between the illumination beams and the normal to the object surface, and $\underline{i}$, $\underline{k}$ are unit vectors along the x,z axes as shown in Figure 8.

These can be substituted into Equation 4, giving

$$g_A \cdot \underline{d} = n_A\lambda \qquad 7$$

$$g_B \cdot \underline{d} = n_B\lambda \; .$$

Their superposition is represented by the difference between these equations

$$n_d\lambda = (g_A - g_B) \cdot \underline{d} \; . \qquad 8$$

Substituting Equations 5 and 6 into 8,

$$n_d\lambda = U(2\sin\alpha) \qquad 9$$

where U is the in-plane displacement component along the longitudinal axis of the beam. Equation 9 is equivalent to Equation 3 which governs the patterns obtained with moire interferometry.

This situation has been investigated previously [7-9] and is classified as holographic-moire analysis. In general, sufficiently large additional phase changes could be introduced between exposures to create high fringe densities in each of the two component patterns (one created by each illumination) so that they interfere and produce holographic moire fringes. However, no additional phase changes have been added to the component patterns in the present investigation, and the holographic fringe patterns (shown in Figures 10 and 11) have insufficient fringe densities to produce the moire effect upon superposition (see Figure 12). However, holographic moire fringes can be constructed graphically as shown in Figure 13 for subsequent comparison with those obtained from high frequency moire interferometry.

Fortunately, the holographic component patterns are not required to make the desired real-time measurements of in-plane displacements. Moreover, they can easily be eliminated by reconstructing the carrier pattern (and each of the initial holograms) using horizontally polarized light (produced by rotating the half wave plate and polarizer in the reference beam). In this case, the vertically polarized object beam and the horizontally polarized reference beam will produce no interference and no real-time holographic interference fringes. However, the initial moire interferometric carrier is still reconstructed holographically. This pattern may then be superimposed on the deformed carrier, which depends only upon the interference between the two object wavefronts diffracted from the specimen in its loaded condition. A similar approach was followed by Chiang and Li [10] in an application to real-time laser speckle photograhy.

Real-time interferometric moire fringes can now be photographed in the image plane as shown in Figure 14. The pattern is indicative of displacement in the U direction (along the longitudinal axis of the beam). Fringe numbers are assigned starting with zero at the top center support and the displacement can be calculated using Equation 7 (f = 2400 lines/mm). As expected, the fringe loci agree well with those constructed in Figure 13.

4. CONCLUSION AND RECOMMENDATIONS

Real-time moire interferograms have been recorded using a holo-camera to store information corresponding to the "undeformed" condition of a structural component. The main advantage of this approach over the earlier double exposure technique is that here the investigator is able to continuously monitor and evaluate full-field displacement during the loading process. This could be extremely important in dynamic situations where a time history must be established, for example, in monitoring crack initiation and growth.

In future research, the visibility of real-time moire fringes could be enhanced using a fiber optic imaging bundle with a resolution sufficient to transmit the moire, but too low to resolve the high frequency carriers. This filtered image could be transferred to a video system for automated analysis.

This procedure (incorporating high resolution photoelectronic recording, data acquisition, digitization, computer-based file manipulation, numerical correlation and graphics display routines) would make quasi-real-time computerized numerical subtraction and/or addition of individual carrier fringe field a possible alternative to optical interference. Interpretation of surface motion could be accomplished after completing an experimental procedure by choosing and numerically comparing any two carrier fringe patterns, as recorded on video tape. This would extend the range over which displacements could be measured and would eliminate the need for subjective evaluations of fringe patterns by investigators.

5. ACKNOWLEDGEMENTS

The authors gratefully acknowledge the support of the Army Research Office (Contract Nos. DAAG 29-84-K-0183 and DAAL 03-86-K-0014), the Center for Applied Optics at the University of Alabama in Huntsville, Marquette University, and AT&T Bell Laboratories. Special thanks are extended to Dan Post and his group at Virginia Polytechnic Institute for their many helpful discussions regarding moire interferometry.

REFERENCES

1. Post, D., Moire interferometry for deformation and strain studies, Optical Engineering, Vol. 24, No. 4, (1985), p. 663-667.
2. Basehore, M. L., Post, D., Displacement fields (U,W) obtained simultaneously by moire interferometry, Applied Optics, Vol. 21, No. 14, (1982), p. 2558-2562.
3. D. Post, R. Czarnek, D. Joh, J. D. Wood, "Shear strain anomalies in composite beam specimens by moire interferometry," Proc. Spring Conference on Experimental Mechanics, Las Vegas, Nevada, June 9-14, 1985.
4. Post, D., Moire interferometry at VPI & SI, Experimental Mechanics, Vol. 23, No. 6, (1983), p. 203-210.
5. Dudderar, T. D., Gilbert, J. A., Real-time holographic interferometry through fiber optics, J. Phys., E: Sci. Instrum., Vol. 18, (1985), p. 39-43.
6. Gilbert, J. A., Dudderar, T. D., Applications of fiber optics to coherent metrology for the study of material deformations and structural mechanics, Army Symposium on Solid Mechanics, Newport, Rhode Island, October 1-3, 1984, p. 63-92.
7. Sciammarella, C. A., Gilbert, J. A., A holographic-moire technique to obtain separate patterns for components of displacement, Experimental Mechanics, Vol. 16, No. 6, (1976), p. 215-220.
8. Hung, Y. Y., Taylor, C. E., Measurement of surface-displacements normal to line of sight by holo-moire interferometry, Journal of Applied Mechanics, Vol. 42, E, No. 1, (1975), p. 1-4.
9. Beranek, W. J., Bruinsma, A. J. A., Determination of displacement and strain fields using dual-beam holographic-moire interferometry, Experimental Mechanics, Vol. 22, No. 9, (1982), p. 317-323.
10. Chiang, F. P., Li, Q. B., Real-time laser speckle photography, Applied Optics, Vol. 23, No. 24, (1984), p. 4469-4470.

APPENDIX

A beam with dimensions shown in Figure 4 was made of PSM-1 (a photoelastic material). After the surface was degreased with isopropanol, roughened with abrasive paper and cleaned with surface conditioner, a thin coat of epoxy was applied to the beam. The epoxied surface was carefully placed face down on the dust free, processed and aluminized photographic plate. After the epoxy cured overnight, the specimen was carefully pried from the plate and excess epoxy in the notched area and along the edges of the beam was removed by hand sanding and/or grinding on a fine grit surface preparation power wheel.

$f = 1/p$ $\sin \alpha = (f/2)\lambda$

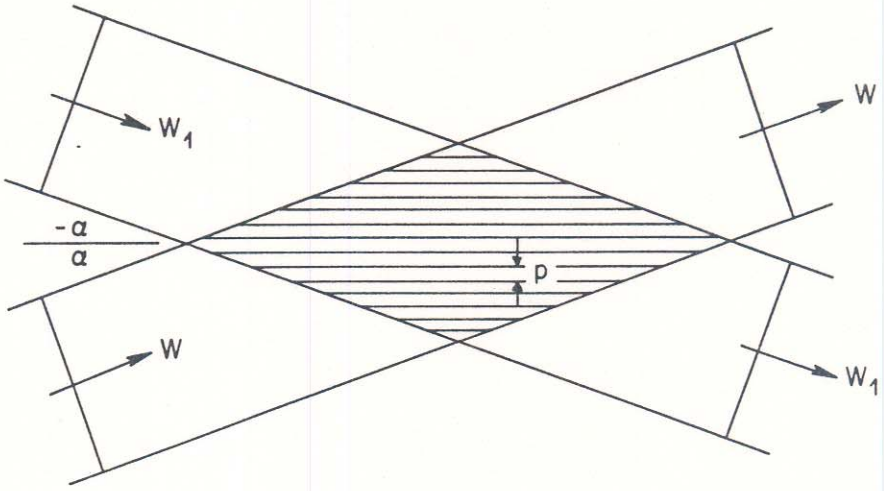

Figure 1. Interference Zone of Two Plane Wavefronts of Coherent Light.

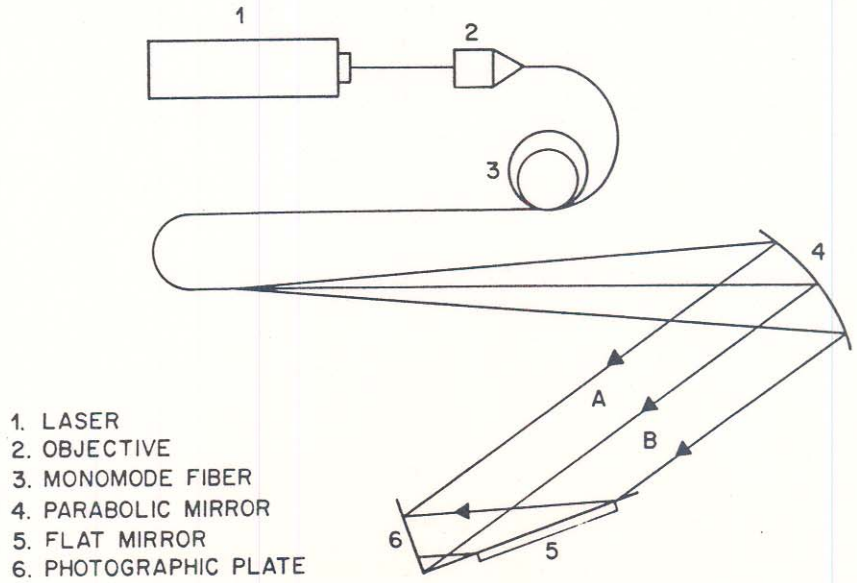

Figure 2. Optical Configuration Used to Produce High Frequency Mold.

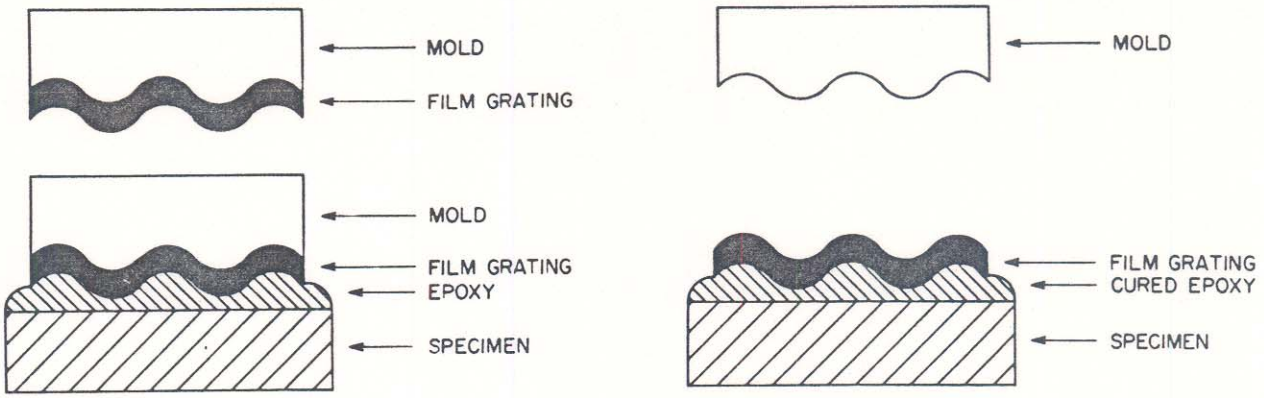

Figure 3. The Grating Transfer from Mold to Specimen Surface.

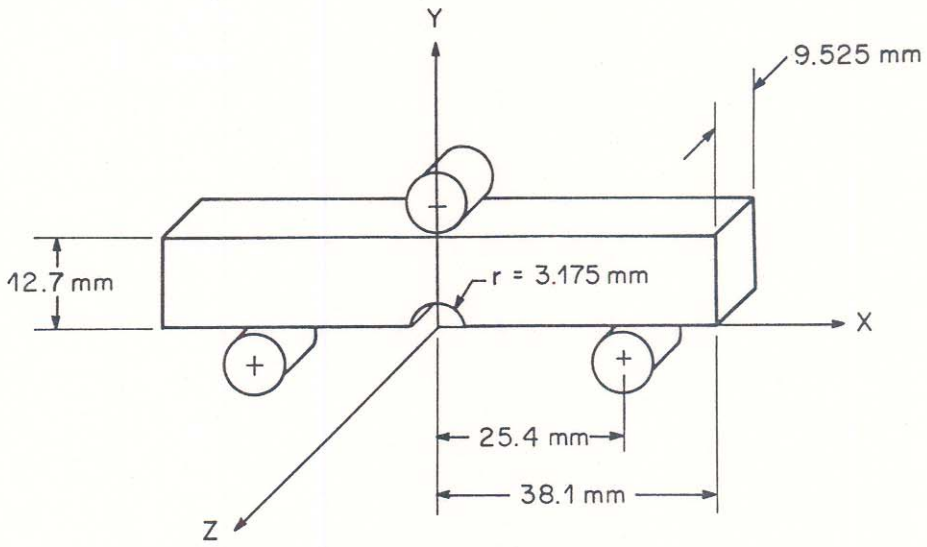

Figure 4. Notched Beam Specimen.

1. LASER
2. BEAM SPLITTER
3. OBJECTIVE
4. OBJECT FIBER
5. REFERENCE FIBER
6. PARABOLIC MIRROR
7. SPECIMEN
8. FLAT MIRROR
9. HALF - WAVE PLATE
10. LINEAR POLARIZER
11. LENS
12. THERMOPLASTIC PLATE
13. IMAGE PLANE

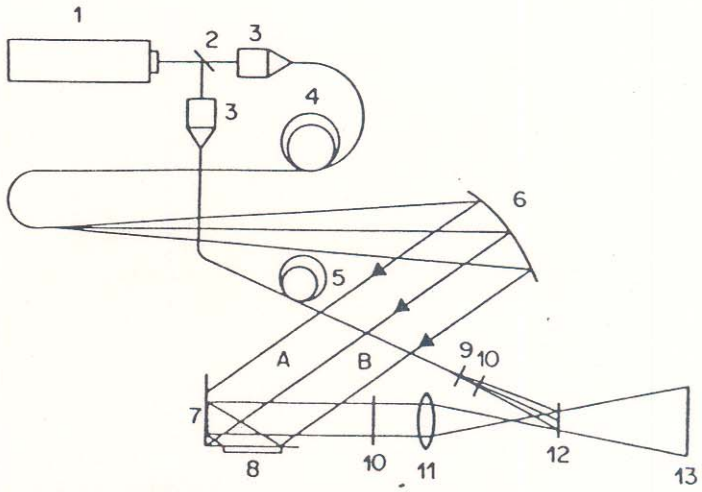

Figure 5. Experimental Set-Up.

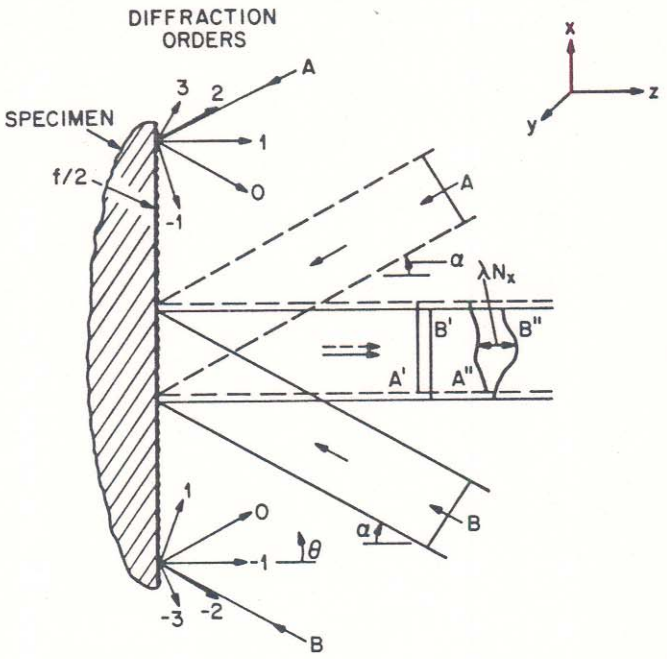

Figure 6. First Order Wavefront Diffraction in Moire Interferometry.

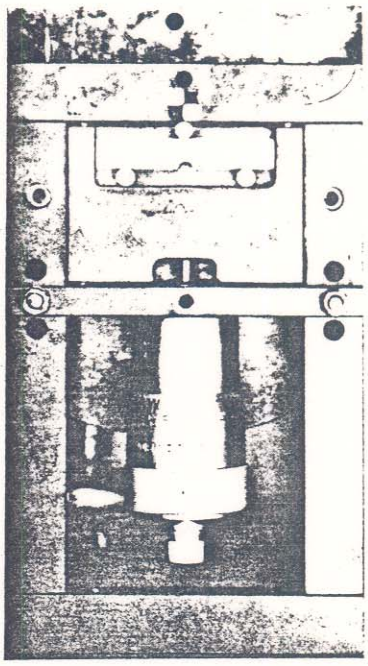

Figure 7. Photograph of Notched Beam in Loading Frame.

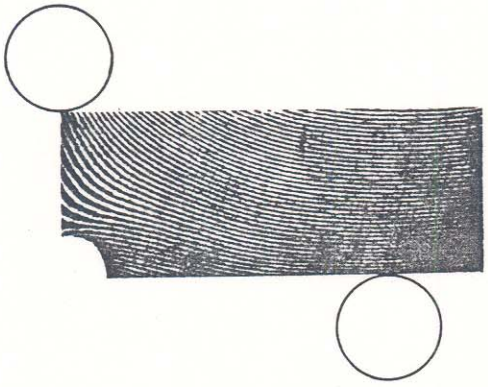

Figure 8. Initial High Frequency Moire Interferometric Carrier Pattern.

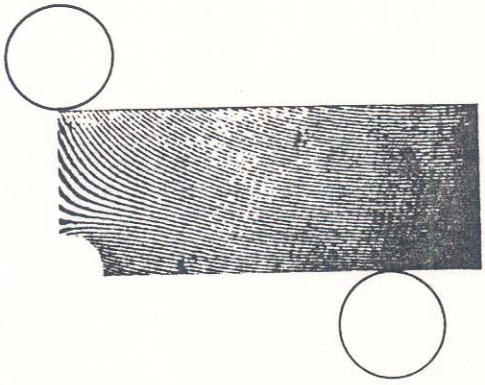

Figure 9. Modulated High Frequency Moire Interferometric Carrier Pattern.

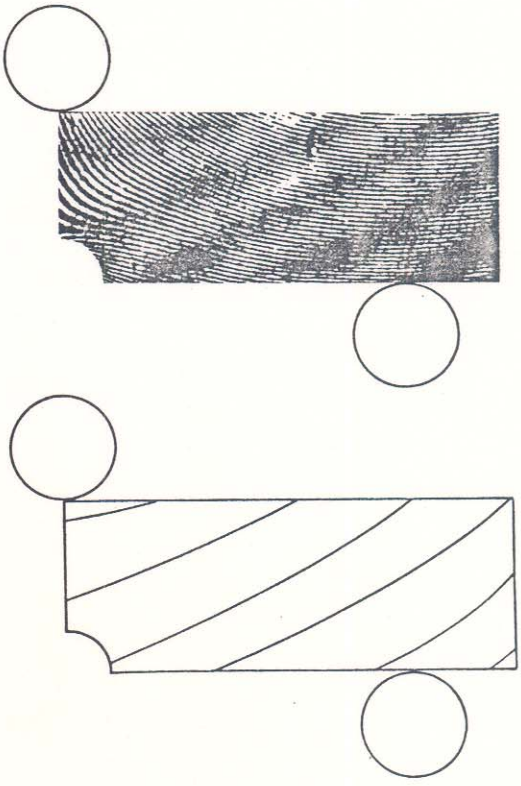

Figure 10. Holographic Pattern Produced by Illumination with Direct Beam A (a) Superimposed on the Initial High Frequency Moire Interferometric Carrier and a (b) Schematic of Holographic Fringe Loci.

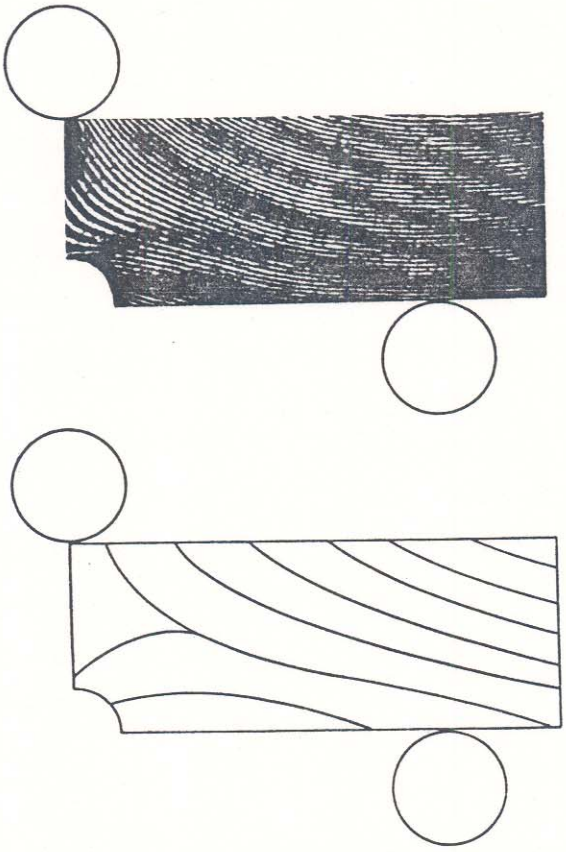

Figure 11. Holographic Pattern Produced by Illumination with Reflected Beam B (a) Superimposed on the Initial High Frequency Moire Interferometric Carrier and a (b) Schematic of Holographic Fringe Loci.

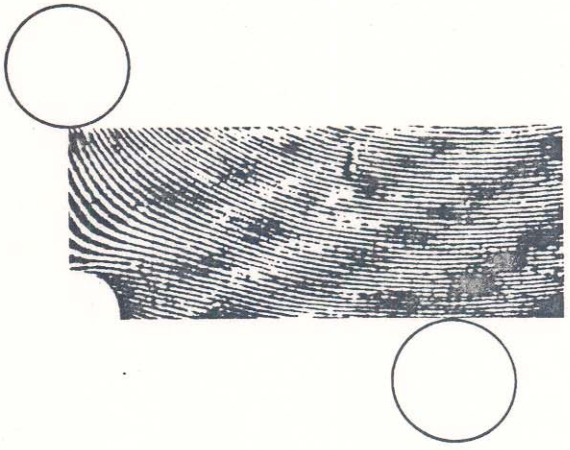

Figure 12. Holographic Pattern Produced by Dual Beam Illumination Superimposed with Initial and Modulated High Frequency Moire Interferometric Carriers.

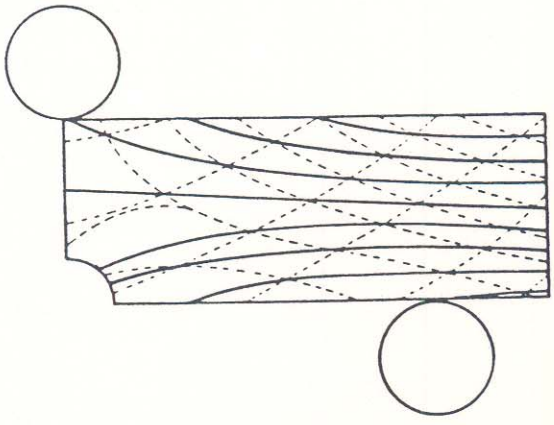

Figure 13. Geometrically Constructed Holographic-Moire Fringes.

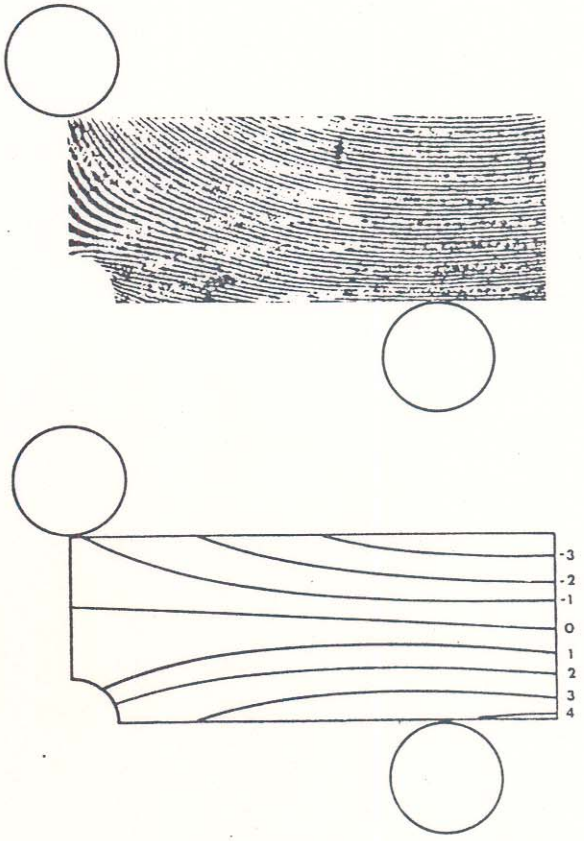

Figure 14. (a) Real-Time Interferometric Moire Pattern and a (b) Schematic of Real-Time Interferometric Moire Fringes.